Catal Lett (2013) 143:844–852
DOI 10.1007/s10562-013-0997-3

Preparation and Photoactivity of Nanocrystalline TiO_2 Powders Obtained by Thermohydrolysis of $TiOSO_4$

A. Di Paola · M. Bellardita · L. Palmisano · R. Amadelli · L. Samiolo

Received: 26 October 2012 / Accepted: 17 March 2013 / Published online: 12 April 2013

Abstract Nanocrystalline TiO_2 photocatalysts were synthesized in mild conditions by thermohydrolysis of $TiOSO_4$ in water at 100 °C and post-calcination treatment at various temperatures. The TiO_2 powders were characterized by X-ray diffraction, X-ray photoelectron spectroscopy, specific surface area determinations, scanning electron microscopy and electron paramagnetic resonance measurements. The photoactivity of the samples was tested employing the photodegradation of 4-nitrophenol in liquid–solid regimen and the photooxidation of gaseous 2-propanol. The best results were obtained with the powder calcined at 600 °C for 10 h. Surprisingly, the not calcined sample was the most active for the abatement of NO_x under irradiation.

Keywords Titanium dioxide · $TiOSO_4$ · Thermohydrolysis · Heterogeneous photocatalysis

A. Di Paola (✉) · M. Bellardita · L. Palmisano (✉)
Schiavello-Grillone Photocatalysis Group, Dipartimento di Energia, Ingegneria dell'informazione, e modelli Matematici (DEIM), Università di Palermo, Viale delle Scienze, 90128 Palermo, Italy
e-mail: agatino.dipaola@unipa.it

L. Palmisano
e-mail: leonardo.palmisano@unipa.it

A. Di Paola · L. Palmisano
Consorzio Interuniversitario La Chimica per l'Ambiente, Via delle Industrie 21/8, 30175 Marghera, Italy

R. Amadelli · L. Samiolo
ISOF-CNR (U.O.S. Ferrara) c/o Dipartimento di Chimica, Università di Ferrara, Via L. Borsari 46, 44121 Ferrara, Italy

1 Introduction

Titanium dioxide currently attracts large interest for its photocatalytic applications in the field of air and water remediation [1–3] and in the field of selective synthesis of chemicals [4–6]. TiO_2 exists in nature in three main polymorphs: anatase (tetragonal), rutile (tetragonal) and brookite (orthorhombic). Anatase is the crystalline structure prevalently used as photocatalyst.

TiO_2 is generally obtained by processes like thermolysis, hydrothermal synthesis and sol–gel routes. The precursors are inorganic or organic Ti(IV) compounds as $TiCl_4$, $TiOSO_4$, and various titanium alkoxides. Regarding economical and practical reasons, $TiCl_4$ is highly toxic and corrosive, the titanium alkoxides are generally very expensive whilst $TiOSO_4$ is a cheap substance so that many papers have concerned the hydrothermal treatment of aqueous $TiOSO_4$ solutions [7–28].

The hydrolysis of $TiOSO_4$ has been widely studied and in particular, the formation mechanism [7, 11], the precipitation procedure [7], and the thermal hydrolysis kinetics [8, 12] have been examined. The effect of post-treatments on the powder morphology [20] and the properties [14] of TiO_2 have been also investigated.

Several parameters affect the photocatalytic activity of TiO_2 and the best results are usually obtained when the catalysts have a high degree of crystallinity and high surface area. Inagaki et al. [22, 28] studied the effect of the crystallinity on the photoactivity of anatase fine powders prepared by hydrolysis of $TiOSO_4$. Enríquez and Pichat [29] showed that the sintering temperature has a different net effect on the photocatalytic removal rate of various organic pollutants in water. The optimisation of the experimental conditions, such as pH, calcination temperature, hydrolysing agent, temperature and ageing time allowed to obtain TiO_2 samples with high activity [15, 16].

Recently, active TiO_2 photocatalysts have been obtained under mild conditions by thermohydrolysis of $TiCl_4$ in pure water at 100 °C [30, 31]. In this study, we report the synthesis of efficient TiO_2 catalysts prepared under similar conditions by thermohydrolysis of $TiOSO_4$ in water at 100 °C. The preparation method is very simple and environmentally friendly since it does not require the use of other reagents [9–20] or relatively high temperatures [21–28]. Many literature publications have studied the behaviour of the photocatalysts toward the degradation of various organic substrates, and comparisons of photoactivities have been made either in an aqueous medium or in the gas-phase. Rarely the activity of a series of photocatalysts was examined in both reaction media. The photocatalytic activity of our samples was evaluated following the photodegradation of 4-nitrophenol in an aqueous solution and the oxidation of 2-propanol in gas–solid regimen. The catalysts were also tested for the abatement of NO_x.

2 Experimental

2.1 Materials

Titanium oxysulfate hydrate ($TiOSO_4 \cdot xH_2O$ Riedel-de Haën), 4-nitrophenol (>99 % Fluka) and 2-propanol (99.8 % Fluka) were used without further purification. Titanium dioxide Degussa P25 (anatase and rutile in the ratio 4:1, specific surface area 50 $m^2\ g^{-1}$) was utilized as provided.

2.2 Samples Preparation

20 g of $TiOSO_4 \cdot xH_2O$ were added to 90 mL of distilled water at room temperature under continuous stirring. The obtained solution was sealed in a bottle and kept in an oven at 100 °C for 48 h. The resultant precipitate was washed by removing many times the supernatant and adding water to restore the initial solution volume. The washing treatment was repeated until residual SO_4^{2-} was not detected by a 0.5 M $Ba(NO_3)_2$ solution. The remaining suspension was dried under vacuum at 55 °C. The powders thus prepared were calcined at different temperatures for 3 h in air.

2.3 Characterization of the Photocatalysts

X-ray diffraction (XRD) patterns of the powders were recorded at room temperature by an Ital Structures APD 2000 powder diffractometer using the Cu Kα radiation and a 2θ scan rate of 2° min. The diffractograms were used to identify the crystal phase and to evaluate the particle sizes by means of the Scherrer equation. The specific surface areas (SSA) of the samples were determined in a Flow Sorb 2300 apparatus (Micromeritics) by using the single-point BET method.

X-ray photoelectron spectroscopy (XPS) analyses were performed with a VG Microtech ESCA 3000 Multilab, equipped with a dual Mg/Al anode. The spectra were excited by the non-monochromatised Al Kα source (1486.6 eV) run at 14 kV and 15 mA.

Scanning electron microscopy (SEM) observations were obtained using a model Philips XL30 ESEM microscope, operating at 25 kV on specimens upon which a thin layer of gold had been evaporated.

2.4 EPR Measurements

EPR spectra were recorded with a X-band Bruker 220 SE spectrometer. Experiments were conducted with suspensions containing the spin trap (1×10^{-1} mol dm^{-3}) that were pre-saturated with O_2 and transferred into a EPR flat cell under an oxygen atmosphere. Photochemical excitation was carried out with light of wavelength above 360 nm directly inside the EPR cavity. All experiments were performed under the same irradiation conditions, i.e., using a Q-400 Hanau medium pressure mercury lamp at a measured light intensity of 5×10^{-3} W cm^{-2}. The quantity of spin trap was established by performing experiments where the signal intensities of the paramagnetic adducts between photogenerated radicals and spin trap were followed as a function of the amount of trap in solution. The used amount of spin trap corresponded to the plateau region. This reasonably ensures that the observed signal due to the adduct is proportional to the amount of radicals produced. Signals were not observed in the dark and in the absence of supported photocatalysts.

2.5 Photoreactivity Experiments

2.5.1 4-Nitrophenol Degradation

A Pyrex batch reactor of cylindrical shape containing 0.5 L of aqueous dispersion was used. A 125 W medium pressure Hg lamp (Helios Italquartz, Italy) was immersed within the reactor and the photon flux emitted by the lamp was $\Phi_i = 11$ mW cm^{-2}. O_2 was continuously bubbled for ca. 0.5 h before switching on the lamp and throughout the occurrence of the photoreactivity experiments. The temperature inside the reactor was ca. 30 °C. The amount of catalyst was 1.2 g L^{-1} and the initial 4-nitrophenol concentration was 20 mg L^{-1}. Samples of 5 mL were withdrawn at fixed intervals of time with a syringe, and the catalyst was separated from the solution by filtration through 0.2 μm Teflon membranes (Whatman). The

quantitative determination of 4-nitrophenol was performed by measuring its absorption at 315 nm.

2.5.2 2-Propanol Oxidation

The photoreactivity runs were carried out in a cylindrical Pyrex batch photoreactor (V = 0.9 L). Thin layers of the powders were prepared by spreading the slurries obtained by mixing the powders with water on glass supports (40 × 40 × 1 mm) that were subsequently dried at 60 °C for 30 min. The samples were irradiated from the top by a 500 W medium pressure Hg lamp. A water filter was placed between the lamp and the photoreactor to cut the infrared radiation. The irradiance at the powder surface was 1.3 mW cm^{-2}. O_2 was fluxed in the reactor for ca. 0.5 h before turning off the inlet and outlet valves. Subsequently, fixed amounts of 2-propanol were directly injected into the reaction chamber and the lamp was switched on. 0.5 cm^3 of the gaseous mixture were withdrawn at different irradiation times using a gas tight syringe and analyzed by gas chromatography.

The photodegradation of 2-propanol was also carried out in a continuous gas–solid reactor. The powders were mixed with water, spread on the walls of a cylindrical Pyrex batch photoreactor (V = 1.5 L) and dried at 60 °C for 30 min. A 500 W medium pressure Hg lamp was used for the irradiation of the catalyst. The photon flux reaching the film surface was 17 mW cm^{-2}. 2-propanol was fluxed into the reactor before irradiation and throughout the duration of the run through a perfusion pump together with a current of oxygen at the flow rate of 300 mL min^{-1}. When the concentration of the substrate was the same in the inlet and in the outlet stream the lamp was switched on.

2-Propanol and propanone concentrations were measured by a GC-17A Shimadzu gas chromatograph equipped with a HP-1 column and a flame ionization detector. CO_2 was detected by a HP 6890 Series GC System equipped with a packed column GC 60/80 Carboxen-1000 and a thermal conductivity detector (TCD). Helium was used as the carrier gas.

2.5.3 NO_X Abatement

The experimental set up for the NO_x abatement has been reported in previous papers [32, 33]. A certain concentration of NO_x was introduced with air in a large volume chamber and after mixing, the gaseous mixture was allowed to circulate through the reaction chamber in the dark, and analysed at established time intervals. Humidity was controlled at 50–60 %. For the photocatalytic tests, the catalyst sample was positioned in the reaction chamber which was provided with an optical window for illumination. An Osram Vitalux lamp was used and the irradiance was 15 mW cm^{-2}. Nitrite and nitrate analysis was carried out by ionic chromatography using a IonPack AS9-HC (25 cm × 4 mm column) and a UV diode detector. The eluent was 9.0 mM Na_2CO_3 in H_2O milli-Q and the flux 1.0 ml min^{-1}.

3 Results and Discussion

3.1 Characterization of the Samples

As shown in Fig. 1, the X-ray diffraction patterns of the powders obtained by thermohydrolysis of $TiOSO_4$ at 100 °C for 48 h were consistent with those of anatase (JCPDS 21-1272). The peaks were rather broad, characteristic of partially crystalline powders with nanosized structure. After thermal treatment for 3 h at different temperatures, the peaks of anatase increased without change of the crystal structure. No peaks of rutile were observed when the powder was treated at 700 °C.

XPS spectra of as-prepared and calcined samples were examined. The Ti 2p spectra showed a peak at 459.5 ± 0.2 eV which is typical of Ti^{4+}. The O 1 s spectra revealed a peak at 532.5 ± 0.2 eV which corresponds to the sulfate (SO_4^{2-}) bonding [20]. As shown in Fig. 2, the existence of sulfate ions

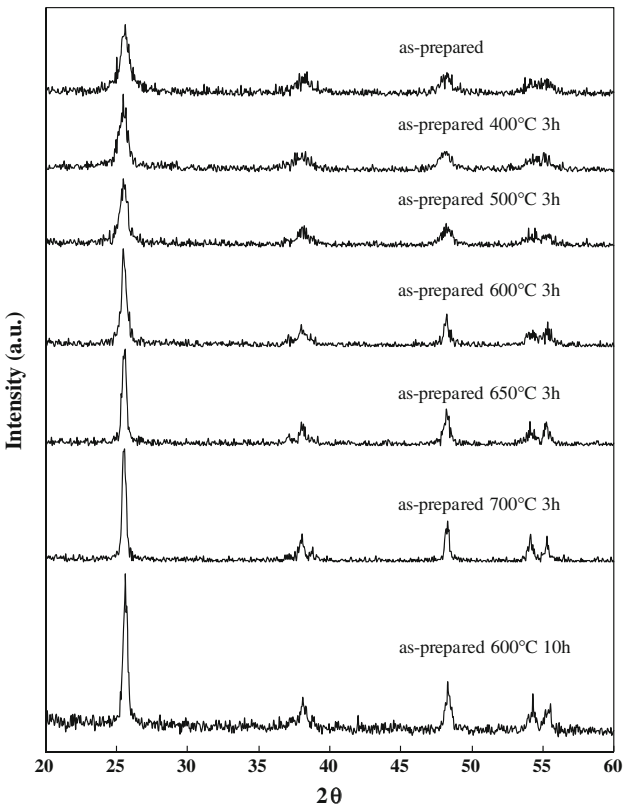

Fig. 1 XRD patterns of the powders obtained by thermolysis of $TiOSO_4$ after heat treatment at different temperatures

leftovers on the surface of TiO_2 was confirmed by the spectra of S 2p which exhibited a binding energy peak of 170.0 ± 0.3 eV. The S/Ti atomic ratios derived from the XPS intensity data (ca. 0.1) were scarcely influenced by temperature and duration of calcination.

The thermal transformation of anatase to rutile has been extensively studied and phase transition temperatures and kinetics around 500–600 °C and 1–50 h have been reported [34–37]. The kinetics of phase change can be modified depending on the preparation conditions [38] and a delay in the phase transition has been observed using surface additives such as the sulfate ions [39]. In the presence of a small amount of $(NH_4)_2SO_4$, the powder obtained by hydrolysis of $TiCl_4$ was completely anatase phase after calcining at 650 °C for 2 h [40] and samples obtained by hydrolysis of $TiOSO_4$ retained the anatase structure after annealing at 600 °C for 1 h [20].

TiO_2 powders obtained by precipitation from a solution of $TiOSO_4$ with NaOH presented pure anatase phase after annealing at temperatures from 300 to 600 °C. A partial transformation to rutile occurred by calcination at 800 °C [16]. Anatase samples synthesized under hydrothermal condition from $TiOSO_4$ aqueous solutions were stable even after annealing at 700 °C for 24 h [22]. Only anatase was identified by treating TiO_2 samples obtained by hydrolysis of $TiOSO_4$ in boiling aqueous solutions of H_2SO_4 and urea at 600 °C for 1 h [14].

The average crystallite sizes of the various powders, determined by means of the Scherrer equation, are reported in Table 1. All the grain sizes were lower than 30 nm and increased with increasing the calcination temperature. The specific surface areas of the samples ranged between 27 and 167 $m^2\ g^{-1}$, and, as expected, decreased with increasing temperature and time of the thermal treatment.

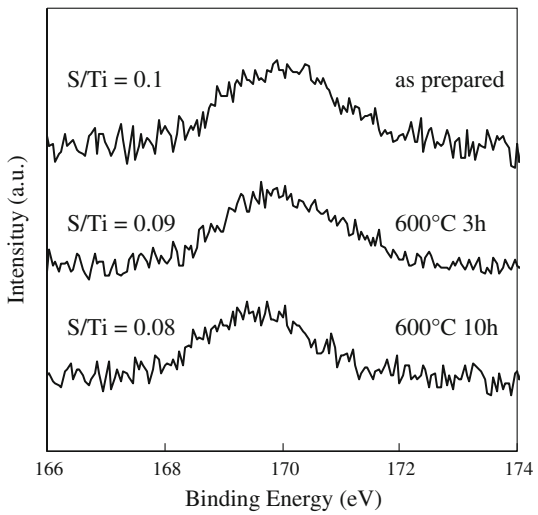

Fig. 2 S 2p XPS spectra of as-prepared and calcined samples

SEM images showed that the samples TiO_2 (as-prepared), TiO_2 (600 °C, 3 h) and TiO_2 (600 °C, 10 h) had similar morphology and the thermal treatment did not alter the structural features and the particles size distribution. A representative SEM micrograph of the as-prepared sample is reported in Fig. 3. The particles were nanostructured with a grape-like shape and higher magnifications revealed that they consisted of aggregates with sizes ranging between 85 and 95 nm.

3.2 EPR Spin-Trapping

Pathways involving holes generally entail the formation of radicals through single electron oxidation processes. However, these radicals are very reactive and their lifetime is too low to be detected by conventional EPR measurements. In this regard, the EPR-spin trapping technique turns out to be a particularly potent tool of investigation because it allows the detection of short lived radical species [41]. This method consists of reactions between short-lived free radicals and diamagnetic nitroso or nitrone compounds used as spin traps. The generated spin adducts have half-lives of the order of several minutes [42] so that they can be measured by conventional EPR spectroscopy. A wide variety of spin traps is available and their reaction with numerous radicals has been extensively investigated [43].

In the present work, we used the EPR spin-trapping technique to investigate the role of the TiO_2 calcination treatment on the formation of OH radicals and of radical intermediates generated in irradiated TiO_2 aqueous suspensions containing 2-propanol. For this purpose we used three different samples: as-prepared, calcined at 600 °C for 3 h and calcined at 600 °C for 10 h.

To detect the OH radicals, experiments were carried out in the presence of 5,5-dimethyl-l-pyrroline-N-oxide (DMPO) which is the most widely nitrone spin trap employed for this purpose [44]. Fig. 4a shows a representative EPR spectrum recorded under irradiation which consists of a 1:2:2:1 quartet with hyperfine splitting constants $a_N = 14.9$ G, $a_H = 14.9$ G. This pattern is characteristic of the DMPO-OH adduct [43, 44] and its signal increases with irradiation time. Compared with the as-prepared sample, the ratios of intensities of the OH signal observed after 3 min of irradiation were 1.2 and 2.5 time higher for the samples calcined at 600 °C for 3 and 10 h, respectively, as shown in Fig. 4b.

Since some doubt has been cast on the mechanism of DMPO-OH formation [45], the formation of radicals in the photooxidation of 2-propanol was also studied using α-phenyl-N-tertbutyl-nitrone (PBN) as spin trap. This compound is reported to be more sensitive to carbon-centered radicals than DMPO [45]. Upon irradiation a spectrum appeared consisting of six lines (a triplet of doublets)

Table 1 Crystallite size (Φ), specific surface area (SSA) and initial reaction rate (r_o) of 4-nitrophenol degradation

Sample	Calcination time (h)	Φ[a] (nm)	SSA[b] ($m^2\ g^{-1}$)	$r_0 \times 10^{9c}$ (mol $L^{-1}\ s^{-1}$)
As-prepared		13	167	11.3
Calcined at 400 °C	3 h	16	121	19.2
Calcined at 500 °C	3 h	18	97	24.2
Calcined at 600 °C	3 h	22	50	37.7
Calcined at 600 °C	10 h	24	44	51.3
Calcined at 650 °C	3 h	24	41	34.1
Calcined at 700 °C	3 h	25	27	35.6
P25			50	38.5

[a] Error: ca. ± 2 %

[b] Error: ca. ± 5 %

[c] All the runs were carried out at pH = 2

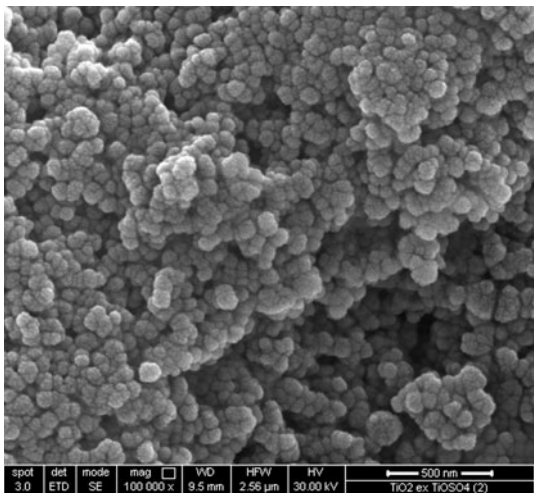

Fig. 3 SEM micrograph of the TiO_2 (as-prepared) sample. Magnification 100,000×

with hyperfine splitting constants $a_N = 15.3$ G and $a_H = 2.7$ G assigned to the PBN-OH adduct [46]. Irradiation of the three selected TiO_2 samples led, in all cases, to the oxidation of the alcohol to hydroxy-alkyl radicals ($R_2^{\cdot}COH$) that were trapped by PBN as inferred from the triplet of doublets with $a_N = 15.5$ G and $a_H = 3.5$ G [44, 47]. The ratios of intensities of the $R_2^{\cdot}COH$ signal were 1.15 and 1.27. It is then apparent that an increase of the calcination temperature and time leads to an enhanced photoreactivity.

Information on hydroxyl radicals generation is important because these species are reported to be the oxidants in the photooxidation reactions on semiconductors. The amount of OH surface groups is expected to be high in the case of the partly crystalline as-prepared sample and to decrease in the samples subjected to increasing calcinations

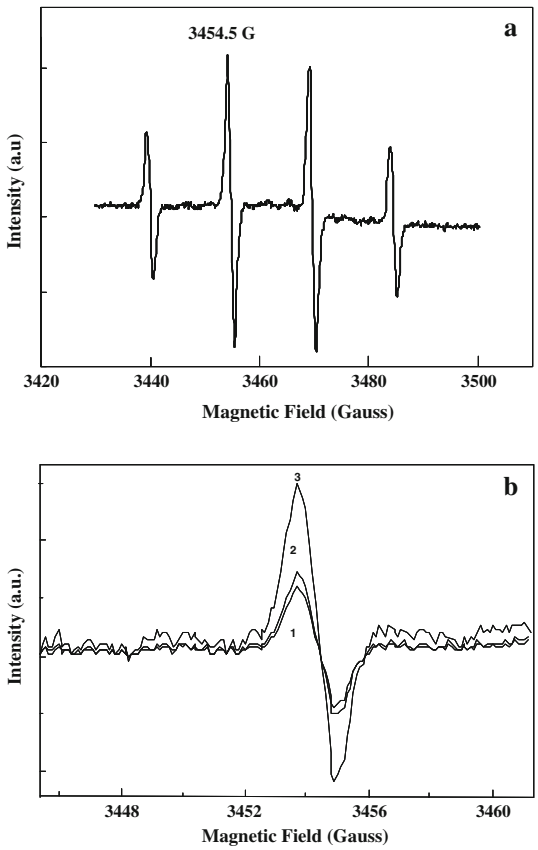

Fig. 4 **a** EPR spectrum of the sample TiO_2 (600 °C, 10 h) obtained under irradiation in the presence of DMPO and **b** details of the signal at 3454.5 G for samples treated at different temperatures: (1) as prepared; (2) 600 °C, 3 h; (3) 600 °C, 10 h

temperatures [48]. The EPR spin trapping results actually reveal the opposite trend and arguably in accordance with the role of OH species, the number of trapped alcohol radicals also increases as post-calcination temperature increases. Nevertheless, it is worth noting that probably the global amount of surface hydroxyl groups cannot be straightforwardly related to the number of photoproduced/trapped OH radicals.

It has been earlier reported that amorphous TiO_2 has negligible photocatalytic activity [49]. Crystallinity is an important photocatalyst property, but partly amorphous commercial catalysts are quite active in the photodegradation of pollutants [50]. Charge recombination, particularly surface recombination, can be sensibly high in poorly crystallized materials [49] due to a large number of defects. Since surface recombination is lower in well-crystallized large particles while bulk recombination is reduced in small particles, particles size and sintering of the photocatalyst have to be optimized [51]. The observed reactivity for the generation of both OH and hydroxyl-alkyl radicals can be explained on the basis of these considerations.

3.3 Photocatalytic Activity

3.3.1 4-Nitrophenol Degradation

The mechanism of the photocatalytic degradation of 4-nitrophenol has been reported in a previous work [52]. The disappearance of 4-nitrophenol was followed by determining the concentration of the substrate at various time intervals. The photoactivity of the various powders was compared with that of commercial Degussa P25 TiO_2. The degradation rate, r_o, referred to a catalyst amount of 1.2 g L^{-1}, was calculated from the initial slope of the concentration versus time profiles. The r_o values are reported in Table 1.

All the powders obtained by thermohydrolysis of $TiOSO_4$ were active for the photodegradation of the substrate. The efficiency of the samples increased with increasing the calcination temperature, reached a maximum and then decreased for temperatures higher than 600 °C.

To study the influence of the heat treatment duration, the as-prepared TiO_2 powder was calcined at 600 °C for 10 h. As shown in Fig. 1, the peaks of anatase increased due to the enhancement of the powder crystallinity. The photoactivity of the sample calcined for 10 h was higher than that exhibited by the sample calcined for 3 h (see Table 1). Similar results were obtained by Inagaki et al. [22, 28] who prepared anatase powders by hydrothermal treatment at 180 °C of aqueous solutions of $TiOSO_4$. The calcined samples with higher crystallinity showed better photocatalytic performance for the decomposition of methylene blue. It is worth noting that the sample obtained after 10 h of calcination at 600 °C was more efficient than Degussa P25 as 4-nitrophenol was completely degraded within ca. 90 min whereas more than 2 h of irradiation were necessary when P25 was used.

3.3.2 2-Propanol Oxidation

The mechanism of the photocatalytic oxidation of 2-propanol by UV illuminated TiO_2 has been already described [53–55]. 2-propanol is decomposed to propanone that is furtherly oxidized to CO_2 [56]. Fig. 5 shows results of the photooxidation of gaseous 2-propanol obtained in the batch reactor under UV irradiation. The amount of substrate introduced into the reactor corresponded to a 74 μM concentration. The samples calcined at 600 °C were very active and, within 180 min, the measured final concentration of CO_2 was three times the initial concentration of 2-propanol confirming that the substrate was completely mineralized. In the presence of the as-prepared sample, less than 40 % of 2-propanol was mineralized after 5 h of irradiation.

Figure 6 shows the results of the photooxidation of 2-propanol obtained in the continuous reactor. In the dark, 2-propanol was increasingly adsorbed until the saturation was reached. When the lamp was switched on, all entering 2-propanol was degraded and converted to CO_2. The outgoing CO_2 concentration was about 50 % of the stoichiometric value indicating that the remaining part of CO_2 was adsorbed on the surface of the catalyst. By injecting H_2O into the reaction chamber the conversion to CO_2 increased since the molecules of water were probably preferentially (photo)adsorbed on the surface sites of TiO_2.

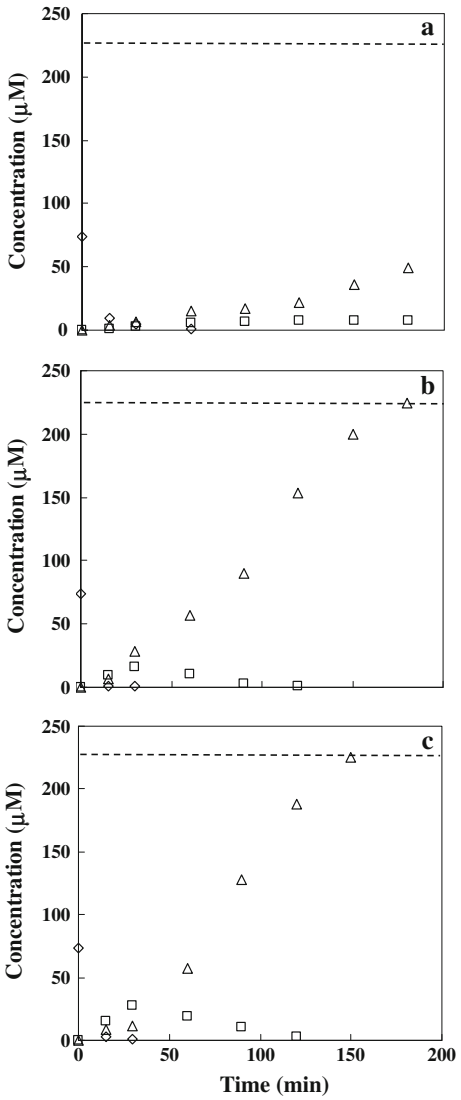

Fig. 5 Photocatalytic degradation of 2-propanol in the batch reactor in the presence of various samples: **a** TiO_2 (as-prepared); **b** TiO_2 (600 °C, 3 h); **c** TiO_2 (600 °C, 10 h). (*diamond*) 2-propanol; (*square*) propanone; (*triangle*) CO_2. $C_0 = 74$ μM. The dashed line corresponds to the stoichiometric amount of CO_2

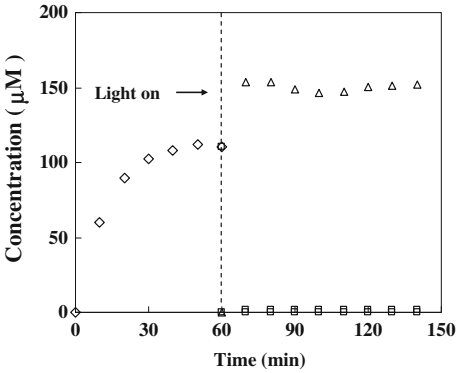

Fig. 6 Photocatalytic degradation of 2-propanol in the continuous reactor in the presence of the sample calcined at 600 °C for 10 h: (*diamond*) 2-propanol; (*square*) propanone; (*triangle*) CO_2. $C_0 = 10^{-4}$ M

3.3.3 Gas-phase Photooxidation of Nitrogen Oxides

Experiments in the absence of catalyst were conducted to assess whether NO_2 underwent photolysis in air:

$$NO_2 \xrightarrow{hv} NO + O \quad (1)$$

but no decrease of NO_2 and corresponding increase of NO was observed.

The photoxidation of a (NO + NO_2) mixture in air is shown in Fig. 7. In contrast to several literature reports which generally refer to nitrogen oxides as NO_x, we distinguished between NO and NO_2 conversion. Figure 7a reveals that the conversion of NO was not much affected by the post-calcination treatment of the photocatalysts. For the conversion of NO_2, the reactivity followed the order:

$$TiO_2\ (\text{as-prepared}) > TiO_2(600^\circ C, 3h) > TiO_2(600^\circ C, 10h)$$

Notably, this sequence of reactivity is inverse compared to that mentioned in the previous sections for the photooxidation of 4-nitrophenol and 2-propanol which seems to correlate with the increase of $OH^\cdot$ radicals as the calcination temperature increases, as evidenced by the EPR data.

The photocatalytic conversion of the nitrogen oxides followed first order kinetics [57]. The experimental rate constants values were 6 (±0.2) × 10^{-4} s^{-1} for the conversion of NO and 4.0 (±0.2) × 10^{-4} s^{-1} (TiO_2 as-prepared) and 2.2 (±0.2) × 10^{-4} s^{-1} (TiO_2 (600 °C, 10 h)), respectively, for the conversion of NO_2. The activity of the sample TiO_2 (600 °C, 3 h) was intermediate between those of the two above samples.

The accepted oxidation pathway can be summarized as follows [57, 58]:

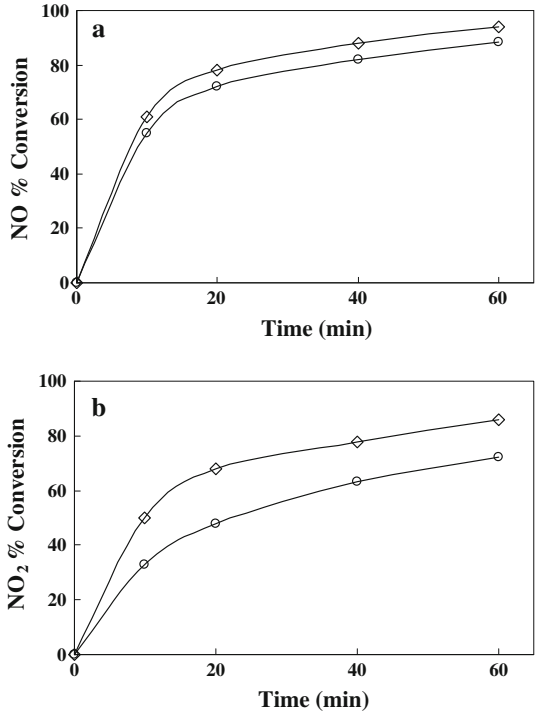

Fig. 7 Photoxidation of a (NO + NO_2) mixture in air: **a** NO conversion, **b** NO_2 conversion (*diamond*) TiO_2 (as-prepared); (*circle*) TiO_2 (600 °C, 10 h)

$$O_2 + e^- \rightarrow O_2^- \quad (2)$$

$$O_2^- + H^+ \rightarrow HO_2^\cdot \quad (3)$$

$$H_2O + h^+ \rightarrow OH^\cdot + H^+ \quad (4)$$

$$NO + O_2^- + H^+ \rightarrow NO_2 + OH^\cdot \quad (5)$$

$$NO_2 + OH^\cdot \rightarrow NO_3^- + H^+ \quad (6)$$

Concerning the mechanism, Laufs et al. [57] proposed that the photocatalytic conversion of NO is initiated by O_2^- (reactions 2, 3 and 5) on the basis of experimental observations such as the need of oxygen to drive the reaction and a lack of sensitivity to humidity and amount of generated OH· radicals (see Sect. 3.2). This conclusion was also arrived at by Hashimoto et al. [48] who proved that indeed NO reacts with O_2^- and that the rate decreases with increasing the calcination temperature due to a decrease in the concentration of the superoxide.

In our system, however, NO conversion is rather insensitive to the post-calcination treatment (Fig. 7a) and, considering that the oxidation proceeds through the reactions 2–6, we are led to conclude that calcination has small effects on the superoxide formation. EPR experiments in dry non-aqueous solvent using DMPO as a spin-trap were also carried out to confirm the involvement of the superoxide. From reported coupling constants [59], we had indeed an evidence of the DMPO-O_2^- adduct formation.

However, a comparison of the data for the different TiO_2 samples was difficult since the spectra are considerably complex being the result of contributions of different species, among which OH· radicals are identified. Detailed studies using more sensitive probes such as luminol [60] might be the object of further investigation.

The photooxidation of NO_2 may likely proceed via reaction (6) on the basis of an observed decrease of the reaction rate in dry conditions, as observed before [60]. However, the conversion efficiency is seemingly in contrast with the observed increase of OH· radicals formation with increasing the calcination temperature (Fig. 7b). Since strong adsorption of NO_2 is observed in the dark, it is plausible that in our conditions the loss of surface area for the thermally treated samples (Table 1) can offset the higher amount of OH· radicals [32].

For the photodegradation of 4-nitrophenol and 2-propanol a key parameter is the decrease in the density of structural defects caused by the calcination, whereas, in the case of the NO_x abatement, the decrease in surface area plays a negative role. These results are in agreement with those of Enríquez and Pichat [29] who evidenced the importance of the molecular structure of the pollutants on the photoactivity of samples obtained by $TiOSO_4$ thermohydrolysis that were calcined at different temperatures.

4 Conclusions

Thermohydrolysis of $TiOSO_4$ in water at 100 °C is an environmentally benign and simple synthetic method to prepare active TiO_2 photocatalysts. Post-calcination treatments allow to increase the crystallinity of anatase which is an important factor in order to get high photocatalytic activity. In agreement with the EPR measurements, the samples calcined at 600 °C were more active than the as-prepared powder for the photodecomposition of 4-nitrophenol in water and the photooxidation of 2-propanol in gas–solid regimen. The sample obtained after 10 h at 600 °C was more efficient than Degussa P25 while the sample not calcined was the most active for the abatement of NO_x, due probably to its higher surface area. Calcination did not significantly affect the photooxidation of NO. In contrast, the conversion of NO_2 decreased by effect of the high temperature treatment.

Acknowledgments The authors thank Dr. Anna Maria Venezia of ISMN-CNR (Palermo) for the XPS measurements.

References

1. Schiavello M (ed) (1988) Photocatalysis and environment, trends and applications. Kluwer Academic, Dordrecht
2. Hoffmann MR, Martin ST, Choi W, Bahnemann DW (1995) Chem Rev 95:69
3. Fujishima A, Rao T, Tryk DA (2000) J Photochem Photobiol C 1:1
4. Palmisano G, Yurdakal S, Augugliaro V, Loddo V, Palmisano L (2007) Adv Synth Catal 349:964
5. Addamo M, Augugliaro V, Bellardita M, Di Paola A, Loddo V, Palmisano G, Palmisano L, Yurdakal S (2008) Catal Lett 126:58
6. Palmisano L, Augugliaro V, Bellardita M, Di Paola A, García López E, Loddo V, Marcí G, Palmisano G, Yurdakal S (2011) ChemSusChem 4:1431
7. Hixson AW, Fredrickson REC (1945) Ind Eng Chem 31:678
8. Santacesaria E, Tonello M, Storti G, Pace RC, Carrà S (1986) J Colloid Interface Sci 111:45
9. Iwasaki M, Hara M, Ito S (1998) J Mater Sci Lett 17:1769
10. Ito S, Inoue S, Kawada H, Hara M, Iwasaki M, Tada H (1999) J Colloid Interface Sci 216:59
11. Sathyamoorthy S, Moggridge GD, Hounslow MJ (2001) Crys Growth Des 1:123
12. Bavykin DV, Savinov EN, Smirniotis PG (2003) React Kinet Catal Lett 79:77
13. Hidalgo MC, Sakthivel S, Bahnemann D (2004) Appl Catal A 277:183
14. Krýsa J, Keppert M, Jirkovský J, Štengl V, Šubrt J (2004) J Mater Chem Phys 86:333
15. Hidalgo MC, Bahnemann D (2005) Appl Catal B 61:259
16. Sakthivel S, Hidalgo MC, Bahnemann DW, Geissen SU, Murugesan V, Vogelpohl A (2006) Appl Catal B 63:31
17. Bavykin DV, Dubovitskaya VP, Vorontsov AV, Parmon VN (2007) Res Chem Intermediat 33:449
18. Grzmil BU, Grela D, Kic B (2008) Chem Pap 62:18
19. Dambournet D, Belharouak I, Amine K (2010) Chem Mater 22:1173
20. Salim NT, Yamada M, Nakano H, Shima K, Isago H, Fukumoto M (2011) Surf Coat Technol 206:366
21. Dai ZM, Chen AP, Yang Y, Gu HC, Gu MY (2001) China Powder Sci Technol 7:14
22. Inagaki M, Nakazawa Y, Hirano M, Kobayashi Y, Toyoda M (2001) Int J Inorg Mater 3:809
23. Kolen'ko YV, Burukhin AA, Churagulov BR, Oleynikov NN (2003) Mater Lett 57:1124
24. Toyoda M, Nanbu Y, Kito T, Himno M, Inagaki M (2003) Desalination 159:273
25. Kolen'ko YV, Churagulov BR, Kunst M, Mazerolles L, Colbeau-Justin C (2004) Appl Catal B 54:51
26. Chuan XY, Hirano M, Inagaki M (2004) Appl Catal B 51:255
27. Hirano M, Ota K (2004) J Mater Sci 39:1841
28. Toyoda M, Nanbu Y, Nakazawa Y, Hirano M, Inagaki M (2004) Appl Catal B 49:227
29. Enríquez R, Pichat P (2006) J Environ Sci Health A 41:955
30. Di Paola A, Cufalo G, Addamo M, Bellardita M, Campostrini R, Ischia M, Ceccato R, Palmisano L (2008) Colloid Surf A 317:366
31. Di Paola A, Bellardita M, Ceccato R, Palmisano L, Parrino F (2009) J Phys Chem C 113:15166
32. Amadelli R, Samiolo L (2007) In: Baglioni P, Cassar L (eds) Photocatalysis, environment and construction materials. RILEM Publications S.A.R.L, Bagneux, pp 155–162
33. Bellardita M, Addamo M, Di Paola A, Marcì G, Palmisano L, Cassar L, Borsa M (2010) J Hazard Mater 174:707
34. Kumar KNP, Keizer K, Bruggraaf AJ, Okubo T, Nagamoto H, Morooka S (1992) Nature 358:48
35. Ding XZ, Liu XH (1997) Mater Sci Eng A 224:210
36. Zhang H, Banfield JF (2000) J Phys Chem B 104:3481
37. Perego C, Revel R, Durupthy O, Cassaignon S, Jolivet JP (2010) Solid State Sci 12:989
38. Ovenstone J, Yanagisawa K (1999) Chem Mater 11:2770

39. Suzuki A, Tukuda R (1969) Bull Chem Soc Jpn 42:1853
40. Zhang Q, Gao L, Guo J (2000) J Eur Ceram Soc 20:2153
41. Amadelli R, Maldotti A, Bartocci C, Carassiti V (1989) J Phys Chem 93:6448
42. Howard JA (1997) In: Alfassi Z (ed) Peroxyl Radicals. Wiley, Chichester, pp 283–334
43. Buettner GR (1987) Free Radic Biol Med 3:259
44. Makino K, Hagiwara T, Murakami A (1991) Radiat Phys Chem 37:657
45. Nosaka Y, Komori S, Yawata K, Hirakawa T, Nosaka AY (2003) Phys Chem Chem Phys 5:4731
46. Amadelli R, Molinari A, Vitali I, Samiolo L, Mura G, Maldotti A (2005) Catal Today 101:397
47. Amadelli R, Samiolo L, Maldotti A, Molinari A, Gazzoli D (2011) Int J Photoenergy. doi:10.1155/2011/259453 Article ID 259453
48. Hashimoto K, Wasada K, Toukai N, Kominami H, Kera Y (2000) J Photochem Photobiol, A 136:103
49. Ohtani B, Ogawa Y, Nishimoto S (1997) J Phys Chem B 10:3746
50. Jensen H, Joensen KD, Jørgensen JE, Pedersen JS, Søgaard EG (2004) J Nanoparticle Res 6:519
51. Zhang Z, Wang CC, Zakaria R, Ying JY (1998) J Phys Chem B 102:10871
52. Di Paola A, Augugliaro V, Palmisano L, Pantaleo G, Savinov E (2003) J Photochem Photobiol A 155:207
53. Harvey PR, Rudham R, Ward S (1983) J Chem Soc Faraday Trans 1(79):1381
54. Ohko Y, Fujishima A, Hashimoto K (1998) J Phys Chem B 102:1724
55. Xu W, Raftery D (2001) J Phys Chem B 105:4343
56. Ohko Y, Hashimoto K, Fujishima A (1997) J Phys Chem A 101:8057
57. Laufs S, Burgeth G, Duttlinger W, Kurtenbach R, Maban M, Thomas C, Wiesen P, Kleffmann J (2010) Atmospheric Environ 44:2341
58. Yen CY, Lin YF, Hung CH, Tseng YH, Ma CCM, Chang MC, Shao H (2008) Nanotechnology 19:045604
59. Brezová V, Gabčová S, Dvoranová D, Staško A (2005) J Photochem Photobiol B 79:121
60. Hirakawa T, Nosaka Y (2002) Langmuir 18:3247